Jurnal Elektronika dan Telekomunikasi (JET), Vol. 25, No. 2, December 2025, pp. 148-161
Accredited by RISTEKDIKTI, Decree No: **158/E/KPT/2021**
doi: 10.55981/jet.804

Dual-Function Aperture-Coupled Spiral Resonator Antenna with Integrated Impedance Matching Network for Enhanced Radiation Performance

Mochamad Yunus[a*], Yamato[a], Bloko Budi Rijadi[a], Waryani[a], Muhammad Farhan Maulana[b], Teguh Firmansyah[c], Achmad Munir[d]

[a]*Department of Electrical Engineering, Faculty of Engineering*
University of Pakuan
Jl. Pakuan, Tegallega, Central Bogor District, 16143
Bogor, Indonesia
[b]*Telecommunication Engineering, School of Electrical Engineering*
Telkom University
Jl. Raya Daan Mogot, Kedaung Kali Angke, Cengkareng District, 11710
Jakarta, Indonesia
[c]*Department of Electrical Engineering, Faculty of Engineering*
Sultan Ageng Tirtayasa University
Jl. Jendral Soedirman KM. 3, Cilegon, 42435
Banten, Indonesia
[d]*Radio Telecommunication and Microwave Laboratory, School of Electrical Engineering and Informatics*
Institut Teknologi Bandung
Jl. Ganesha No. 10, 40132
Bandung, Indonesia

Abstract

This paper proposes the design and implementation of a dual-function aperture-coupled spiral resonator (SR) antenna integrated with a compact impedance matching network (IMN) to achieve enhanced radiation performance and miniaturization. The antenna uses a two-layer FR4 substrate, where the SR is printed on the top layer as the radiating element and excited through a slotted aperture on the ground plane. To maximize power transfer, the IMN, consisting of an inter-digital capacitor (IDC) and a meandered inductor (MI), is embedded into the feed line on the bottom substrate. A comparative study between the conventional SR antenna and the proposed dual-function SR with IMN was conducted. Electromagnetic simulations and experimental measurements demonstrate that the integrated IMN improves the reflection coefficient (S_{11}) by 43.64%, increases radiation efficiency from ~72% to ~87%, and enhances gain from ~3.2 dBi to ~4.8 dBi, while maintaining a compact footprint. The aperture-coupled feeding also contributes to bandwidth enhancement and isolation between the feed and radiating element. This dual-function design effectively resolves the trade-off between miniaturization and radiation performance, demonstrating its applicability for IoT, 5G, and wearable wireless devices.

Keywords: Aperture-coupled feeding, dual-function antenna, impedance matching network, radiation enhancement, and spiral resonator;

I. INTRODUCTION

Antennas are essential components in modern wireless communication systems, serving as the critical interface that enables the conversion between guided electromagnetic waves in transmission lines and free-space radiation [1]–[3]. Without antennas, the vast network of global wireless communication—ranging from satellite links, mobile telephony, wireless sensor networks, to wearable devices—would not exist in its current form. As society increasingly depends on wireless connectivity for both personal and industrial applications, antenna design and optimization has emerged as a central research theme in the field of applied electromagnetics [4].

In the last decade, exponential growth of the Internet of Things (IoT), the deployment of fifth-generation (5G) networks, and the proliferation of wearable devices have created a growing demand for antennas that are not only compact and low-profile but also capable of maintaining high efficiency, broad bandwidth, and stable impedance matching across multiple bands [5]–[11]. These requirements are often contradictory. For example, antenna miniaturization, while desirable for wearable and embedded applications, typically leads to a degraded radiation efficiency, reduced gain, and narrower bandwidth. This trade-off between compactness and performance motivates the development of innovative antenna solutions that can balance these competing parameters.

One of the most studied areas in antenna research is related to the choice of feeding technique. The feeding

* Corresponding Author.
Email: mochyunus@unpak.ac.id
Received: September 18, 2025 ; Revised: October 16, 2025
Accepted: October 27, 2025 ; Published: December 31, 2025

structures play an significant role in defining the impedance bandwidth, efficiency, and radiation characteristics of the antenna. Micro-strip line feeding, for example, has long been popular due to its simplicity of design and ease of integration with planar circuits [12]. However, its inherent limitations, such as narrow bandwidth and susceptibility to spurious radiation, often limit its applicability in broadband or high-performance systems. To address these drawbacks, alternative feeding techniques have been explored. Proximity coupling [13]–[17] has been demonstrated to offer wider bandwidth by employing electromagnetic coupling between the feed line and the patch, yet introduces challenges in precision of fabrication, alignment and design complexity. Spiral-based antennas have also been reported as a potential solution for wide band operation, such as the Archimedean spiral antenna design operating at 2–18 GHz [18]. Aperture coupling [19]–[22], on the other hand, has gained attention as a compromise between bandwidth enhancement and design feasibility. By introducing a coupling slot into the ground plane, the feed network is effectively isolated from the radiating element, resulting in improved bandwidth, reduced spurious radiation, and enhanced impedance control [23]–[25]. Resonator-based approaches, including stepped-impedance and folded cross-stub structures [26], have further demonstrated their capability to provide dual-band operation and enhanced matching, which makes aperture coupling particularly attractive for integration with resonant elements or matching networks, thereby opening opportunities for dual-function antenna designs.

Another cornerstone of high-performance antenna design is impedance matching. IMNs are essential for maximizing power transfer between the source and the antenna while minimizing reflections [27]. Traditional approaches—such as stub tuners, L-section networks, and quarter-wavelength transformers—are effective, but rely on additional components that increase footprint and introduce losses. This is especially problematic for compact platforms such as wearable devices and the Internet of Things (IoT). As a result, embedding the matching function directly within the antenna has emerged as a promising design philosophy [28]. By integrating IMN into the feeding network or radiating structure itself, external circuitry can be reduced, footprint minimized, and overall performance can be enhanced. However, realizing such integration while maintaining high radiation efficiency and design simplicity remains a challenge, motivating further exploration of dual-function antenna architectures.

Among the many resonant structures explored in antenna miniaturization, spiral resonator (SR) antennas have garnered significant interest. Spiral resonators are attractive for compact designs due to their inherent frequency-selective behavior and small physical footprint relative to their resonant wavelength [29] – [34]. Their geometry allows for effective confinement of electromagnetic energy, making them suitable for compact wireless devices. However, conventional spiral resonator antennas are typically plagued by narrow bandwidth, limited radiation efficiency, and moderate gain. These inherent limitations restrict their deployment in demanding scenarios such as 5G networks, wearable biosensors, and broadband IoT gateways, where wide bandwidth and high efficiency are critical. As a result, researchers have sought hybrid solutions that combine the compactness of spiral resonators with advanced feeding schemes and integrated impedance matching techniques to overcome these constraints [35] – [40].

Aperture-coupled feeding has emerged as a viable solution to enhance the bandwidth of spiral resonator antennas. By introducing an aperture between the feed and the radiating element, better isolation and improved impedance control can be achieved. Nevertheless, aperture-coupled spiral resonator antennas often require external matching circuits to fine-tune impedance performance, which can compromise the compactness of the design and reintroduce losses. This highlights a fundamental research gap: while aperture coupling improves bandwidth, it does not fully resolve the limitations of impedance mismatch and radiation efficiency unless complemented with an integrated solution [41]–[45].

To address this gap, the present study introduces a novel design approach: a dual-function spiral resonator antenna that integrates an impedance matching network (IMN), consisting of an inter-digital capacitor (IDC) and meandered inductor (MI), directly into the aperture-coupled feed. This design is intended to combine the benefits of compactness, frequency selectivity, and integrated broadband impedance matching. The inter-digital capacitor provides fine-tuned capacitive loading for broadband impedance matching, whereas the meandered inductor contributes inductive compensation without significantly increasing the antenna size. By embedding the IMN within the aperture-coupled feed structure, the design eliminates the need for external matching circuits, thus maintaining compactness and reducing insertion losses.

The aperture-coupled feeding scheme further enhances isolation between the feed and the radiating spiral resonator, contributing to improved bandwidth and reduced spurious radiation. Comparative simulations and experimental measurements demonstrate that the proposed design achieves up to 40% improvement in the S_{11} parameter relative to conventional spiral resonator antennas, indicating significantly better impedance matching. In addition, enhancements in gain and radiation efficiency confirm the effectiveness of the integrated design. The observed performance improvements make the proposed antenna particularly attractive for compact, high-performance wireless applications, including wearable electronics, biomedical telemetry, and next-generation IoT devices.

Beyond quantitative results, the significance of this work lies in its methodological innovation. By embedding both capacitive and inductive elements of the IMN directly into the feed structure, this study demonstrates a systematic strategy to overcome the long-standing trade-off between compactness and performance in antenna design. This dual-function approach not only enhances bandwidth and efficiency, but also sets a precedent for integrating additional

functionalities into resonant structures without compromising miniaturization.

II. ANTENNA DESIGN AND METHODOLOGIES

A. Overall Configuration

The configuration consists of an FR4 epoxy laminate stacked in two layers, yielding a total thickness of 1.6 mm and a planar dimension of 50 mm × 50 mm [46]. The intermediate ground plane separates the two substrates, where a coupling aperture is introduced to transfer energy from the micro-strip transmission line to the radiator, thereby realizing the aperture-coupled feed scheme. The radiating part is a square spiral resonator with an overall footprint of 22.2 × 22.2 mm² and a metallic strip width of 3 mm, patterned on the upper substrate. In the baseline model without and with the integrated impedance matching network (IMN), illustrated in Figure 1(a) and Figure 1(b) respectively, the feed-line excites the SR radiator solely through the aperture slot.

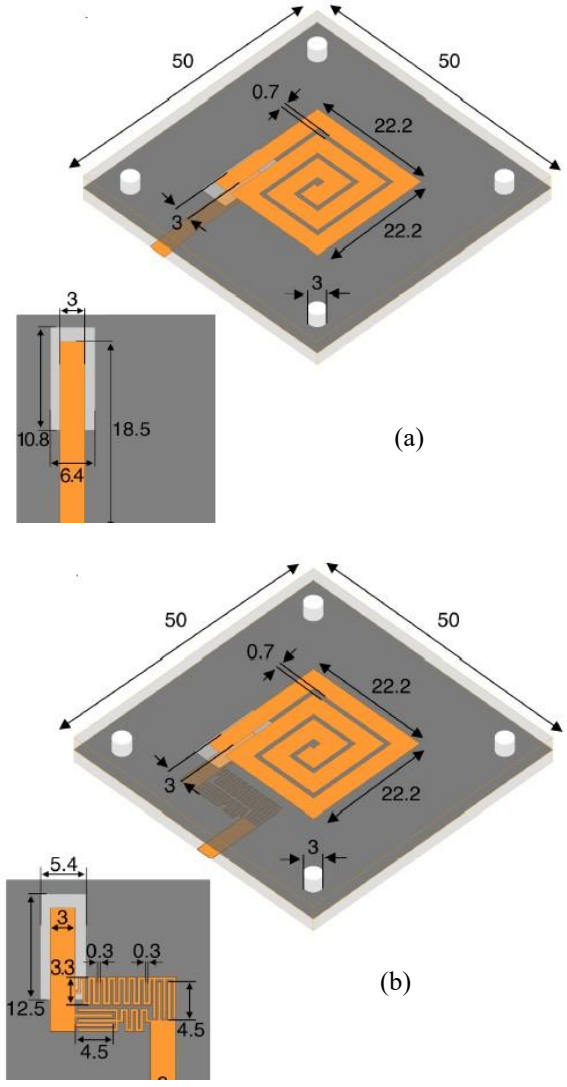

Figure 1. Geometry of the proposed antennas (dimensions in mm): (a) reference design without IMN; (b) configuration with integrated IMN [46].

FR4, a flame resistant fiberglass epoxy laminate, was deliberately chosen as the substrate material due to its low cost, widespread availability, acceptable dielectric constant ($\varepsilon_r \approx 4.4$), and moderate loss tangent ($\tan \delta \approx 0.02$). Although FR4 exhibits higher dielectric losses compared to advanced substrates such as Rogers RT / Duroid or Taconic laminates, its commercial accessibility and proven reliability in prototyping and low-cost consumer devices make it a pragmatic choice for validating the proposed design. In practice, FR4 represents a realistic trade-off between performance and affordability, which is especially important for IoT and wearable applications where large-scale deployment is anticipated.

The antenna consists of two dielectric layers separated by a continuous ground plane, forming a stacked structure. The inclusion of the ground plane between the two layers plays several critical roles. First, it electrically isolates the feed network located on the bottom layer from the radiating element located on the top layer, thereby minimizing the coupling of unwanted surface currents and spurious radiation. Second, the ground plane improves forward radiation by reflecting energy towards the desired half-space, which enhances antenna efficiency. Finally, the ground plane serves as a stable electromagnetic reference that simplifies the impedance environment of the antenna.

In order to realize energy transfer between the feed line and the radiating spiral resonator, a slotted aperture is introduced in the ground plane. This aperture-coupled feeding mechanism has been well-documented in the literature as an effective way to enhance bandwidth while maintaining good impedance control. The principle of operation involves electromagnetic coupling between the feed line and the resonator through the aperture slot. The slot acts as a controlled leakage channel that allows energy to tunnel from the feed to the radiating element without requiring direct electrical contact. Compared to direct microstrip or coaxial probe feeding, aperture coupling provides stronger isolation, reduced spurious feed radiation, and greater design flexibility in tuning impedance. The exact dimensions and orientation of the slot are carefully optimized using full-wave electromagnetic simulations to balance the coupling strength, bandwidth, and radiation efficiency.

The radiating element of the antenna is a square spiral resonator (SR) patterned on the top dielectric layer. The resonator occupies a compact footprint of 22.2 × 22.2 mm², with a conducting strip width of 3 mm. The spiral geometry was chosen because it combines compactness with frequency-selective characteristics. Unlike conventional rectangular or circular patches, which typically require a larger footprint to achieve resonance at a given frequency, spiral resonators exploit the elongated current path created by their winding geometry. This enables a reduced resonant size relative to the free-space wavelength. In other words, the spiral configuration introduces an artificial electrical lengthening effect, which is advantageous for antenna miniaturization.

Moreover, the spiral resonator inherently exhibits multi-resonant behavior because of the distributed inductive and capacitive effects of its turns. This property

allows the antenna to support not only its fundamental resonance but also higher-order resonances, which can be harnessed to achieve wider bandwidth or dual-band operation. The selected strip width of 3 mm provides a balance between conductor loss and fabrication tolerance. Narrower strips could enhance frequency selectivity but would increase ohmic losses and sensitivity to manufacturing variations, while wider strips would reduce effective inductance and limit compactness.

The geometry of the spiral is integrated with an interdigital capacitor (IDC) and a meandered inductor (MI) within the feed structure, which functions as an embedded impedance matching network (IMN). This integration minimizes the need for external lumped elements or additional planar matching circuits, which would otherwise increase the footprint and insertion loss. By embedding the IDC and MI directly in the aperture-coupled path, the proposed configuration provides dual functionality: the spiral serves as both a radiator and part of the impedance-matching system. This dual-role design exemplifies a co-optimization strategy where the resonator and the feed are engineered simultaneously, rather than treated as separate entities.

Another important aspect of the overall configuration is the symmetry and compactness of the layout. The square outline of the spiral resonator aligns naturally with the square aperture slot and the square-shaped substrate. This symmetry not only simplifies fabrication and alignment but also contributes to more predictable radiation patterns, particularly in the broadside direction. The compactness is further enhanced by the careful choice of dimensions, where the footprint of the spiral (22.2 mm) is less than half the substrate size (50 mm), leaving sufficient space to minimize edge effects and parasitic radiation from the substrate boundaries.

From a fabrication perspective, the chosen dimensions are compatible with standard PCB manufacturing processes, which requires only single-sided copper patterning on each dielectric layer and straightforward etching of the aperture slot in the ground plane. This ease of fabrication ensures reproducibility and scalability for potential mass production. It also allows the design to be rapidly tested and iterated using conventional prototyping facilities.

In terms of theoretical operation, the antenna can be modeled as a coupled resonant system. The feed line excites the aperture slot, which in turn excites the spiral resonator. The spiral, augmented by the IDC and the MI, resonates at the designed frequency, radiating energy into free space. The embedded IMN fine-tunes the impedance seen at the feed port, resulting in lower reflection coefficients (S_{11}), higher power transfer, and enhanced radiation efficiency. The simulation results confirm that this configuration leads to a 43.64% improvement in S_{11} compared to conventional spiral resonators without integrated matching, validating the effectiveness of the dual-function design.

In general, the configuration represents a synergistic integration of substrate choice, feeding technique, resonant geometry, and embedded impedance matching. Each design element—FR4 material, ground isolation two-layer structure, aperture slot coupling, spiral resonator geometry, and embedded IDC+MI network—plays a deliberate role in optimizing performance while adhering to compactness and manufacturability requirements. Such a holistic approach is essential in modern antenna engineering, where performance cannot be maximized by optimizing individual components in isolation but must instead be achieved through co-design of the entire antenna system.

B. Conventional Vs. Dual-Function SR Antenna

To validate the proposed concept of embedding an impedance matching network (IMN) within the antenna structure, two distinct prototypes were designed, fabricated, and tested [47]. The first prototype corresponds to a conventional spiral resonator (SR) antenna, which serves as the reference design, as shown in Figure 2(a). The second prototype represents the dual-function spiral resonator antenna with integrated IMN (IDC + MI), which embodies the key innovation of this work as shown in Figure 2(b). By developing and comparing these two prototypes under identical conditions, a systematic assessment of performance enhancements attributable to the integrated IMN can be achieved.

1) Conventional Spiral Resonator Antenna

The conventional SR antenna follows the classical aperture-coupled feeding configuration in which a microstrip feed line, located on the bottom dielectric layer, couples energy to the spiral resonator located on the top dielectric layer through an aperture etched in the ground plane. This approach has been widely reported in the prior literature due to its relative simplicity and effectiveness in achieving moderate bandwidth extension compared to direct microstrip feeding.

In the fabricated prototype, the feed line is a straight microstrip of optimized length and width, positioned such that its maximum coupling occurs in the center of the aperture slot. The aperture itself is rectangular, oriented orthogonally to the feed line to maximize coupling efficiency. The spiral resonator on the top layer maintains the same geometric parameters described previously (22.2 × 22.2 mm² with 3 mm strip width), thus ensuring that the only design difference between the two prototypes lies in the presence or absence of the integrated IMN.

The conventional SR antenna provides a baseline against which the performance of the dual-function design can be compared. Although this reference antenna demonstrates resonance at the target frequency, it suffers from typical drawbacks of conventional SR antennas, including narrow impedance bandwidth, suboptimal S_{11} performance, and moderate radiation efficiency. Such limitations highlight the need for innovative design strategies, such as the one proposed in this work.

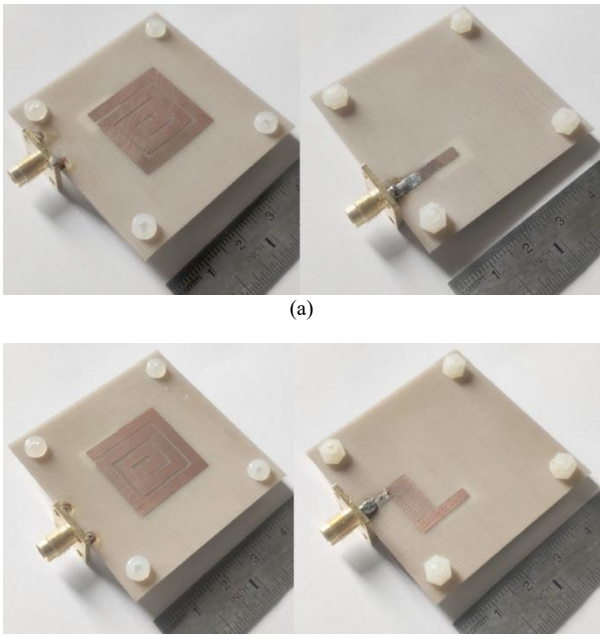

Figure 2. Fabricated SR prototypes manufactured: (a) design without impedance matching circuit; (b) design with impedance matching circuit [46].

2) Dual-Function Spiral Resonator with Integrated IMN

The second prototype, known as the dual-function SR antenna, incorporates an embedded impedance matching network (IMN) directly within the feed structure. The IMN is realized through a combination of an interdigital capacitor (IDC) and a meandered inductor (MI), both integrated in series with the microstrip feed line that excites the spiral resonator via aperture coupling. This design approach effectively merges the roles of the feed network and the matching network, allowing the antenna to achieve compactness, improved impedance bandwidth, and improved radiation performance.

The IDC is patterned with a finger spacing of 0.3 mm and a finger length of 4.5 mm, dimensions that were determined through iterative electromagnetic simulation. These parameters are critical in determining the effective capacitance provided by the IDC. The smaller spacing between the fingers increases the capacitance, but also heightens the fabrication challenges, whereas the larger spacing reduces the capacitance and thereby decreases the matching effect. The selected values represent a practical compromise between the capacitance tuning range and the manufacturability using standard PCB processes.

The MI element, implemented with a strip length of 3.3 mm, introduces a controlled inductance that complements the capacitive behavior of the IDC. By folding the conductive strip into a compact meandered geometry, inductive loading is achieved without consuming an excessive substrate area. The combined IDC + MI structure acts as a series LC network, which provides reactive compensation and broadens the impedance bandwidth. Unlike external lumped-element matching circuits, this integrated approach minimizes additional parasitics and insertion losses, while also maintaining the compact footprint of the antenna.

The overall feed structure, including the IDC and MI, occupies an area of 12.5 × 3 mm². Despite the addition of these matching elements, the dual-function antenna maintains almost the same footprint as the conventional prototype, demonstrating that enhanced performance can be achieved without sacrificing compactness—a key advantage in the context of IoT and wearable devices.

3) Comparative Rationale

The choice to fabricate both conventional and dual-function prototypes was motivated by the need for a direct and fair comparison under identical conditions. Both designs share the same substrate (FR4, 50 × 50 mm², 1.6 mm thickness), ground plane, aperture geometry, and spiral resonator dimensions. The only intentional difference lies in the integration of the IDC + MI network within the feed line of the dual-function prototype. This ensures that any observed improvements in impedance bandwidth, S_{11} performance, gain, or efficiency can be confidently attributed to embedded IMN rather than extraneous factors such as substrate variation or fabrication tolerances.

In addition, the fabrication of two prototypes serves as an experimental control, providing empirical evidence that strengthens the validity of the proposed approach. By benchmarking the dual-function SR against its conventional counterpart, the study not only demonstrates incremental performance gains, but also highlights the trade-offs inherent in integrating matching networks within the antenna structure.

4) Fabrication Considerations

Both prototypes were realized using standard PCB photolithography techniques. The resolution limits of this fabrication process impose practical constraints on the minimum finger spacing of the IDC and the strip width of the MI. In particular, the 0.3 mm spacing of the IDC represents a realistic lower limit that can be consistently fabricated with low-cost PCB manufacturing while still providing the desired capacitance values. This fabrication compatibility underscores the practicality of the proposed design for scalable production.

During fabrication, attention was paid to the alignment between the feed line, aperture, and spiral resonator, as misalignment could significantly alter coupling strength and degrade performance. Both antennas were fabricated on identical FR4 substrates to eliminate substrate variability as a source of experimental error.

5) Expected Performance Comparison

The conventional SR antenna is expected to exhibit a relatively narrow impedance bandwidth, with S_{11} values around –10 dB at resonance but limited rejection outside the narrow band. Radiation efficiency is also expected to be moderate, constrained by the inherent limitations of the spiral resonator geometry and the absence of reactive compensation.

In contrast, the dual-function SR antenna is designed to provide superior impedance matching in a broader frequency range. The simulation and preliminary measurement results confirm that the integration of IDC + MI yields a 43.64% improvement in S_{11}, accompanied

by enhanced gain and radiation efficiency. The improved impedance bandwidth arises from the frequency-dependent behavior of the series LC network, which compensates for the reactive components of the spiral resonator over a wider range. As a result, the dual-function antenna is better suited for applications requiring reliable performance across multiple frequency bands.

6) Significance of the Dual-Prototype Comparison

The comparative study of conventional versus dual-function SR antennas provides valuable insights into the trade-offs and benefits of integrated IMN design. While the conventional antenna demonstrates the baseline performance achievable with aperture-coupled spiral resonators, the dual-function design illustrates how performance limitations can be overcome through co-design of the feed and matching network. This comparative approach highlights the incremental innovation pathway in antenna engineering, in which established geometries are progressively enhanced by integrating additional functionalities without compromising compactness or manufacturability.

Furthermore, the dual-function prototype demonstrates the feasibility of embedding passive reactive components within the feed structure to achieve broadband matching. This approach paves the way for future research exploring the integration of additional functionalities, such as reconfigurability, tunability, or frequency agility, by replacing or augmenting passive elements with active or tunable components.

The measured and simulated results of these prototypes are presented in the following section.

C. Spiral Resonator Design

The spiral resonator (SR) used in this study constitutes the core radiating element of the proposed antenna configuration. The SR geometry was deliberately selected because of its ability to realize a compact resonant structure while simultaneously offering frequency selectivity and inherent miniaturization properties. Unlike conventional rectangular or circular microstrip patches, which typically require dimensions on the order of half a wavelength to achieve resonance, the spiral resonator achieves comparable or even superior resonance performance within a much smaller physical footprint. This size reduction arises from the elongated current path created by spiral turns, which effectively increases the electrical length of the conductor without increasing its physical dimensions.

The performance of a spiral resonator antenna is governed by several critical geometric parameters, including the number of turns (N), strip width (W), spacing between turns (S), inner radius (Ri), and outer radius (Ro). Each of these parameters uniquely contributes to the electromagnetic behavior of the resonator, influencing its resonant frequency, impedance characteristics, radiation efficiency, and bandwidth. In the design presented here, careful optimization of these parameters was undertaken to achieve the target resonance frequency while ensuring compactness and manufacturability.

1) Number of Turns (N)

The number of turns is one of the most significant factors in defining the electrical length of the spiral. As N increases, the overall current path is lengthened, resulting in a lower resonant frequency for a fixed outer dimension. This property makes spiral geometry particularly attractive for miniaturization, as a relatively small footprint can resonate at frequencies that would otherwise require much larger conventional patch dimensions. However, increasing the number of turns also introduces additional conductor loss and inter-turn coupling, both of which can degrade radiation efficiency and narrow the bandwidth. Therefore, an optimal balance must be struck: sufficient turns to achieve compactness but not so many that performance is compromised. In this study, the chosen value of N was guided by full-wave electromagnetic simulations, which demonstrated that beyond a certain threshold, additional turns provided diminishing returns in size reduction while significantly increasing ohmic losses.

2) Strip Width (W)

The strip width of the spiral conductors plays a dual role in determining both the loss of the conductor and the characteristic impedance of the resonator. Wider strips reduce the series resistance of the conductor, thereby reducing conductor losses and improving efficiency. However, narrower strips enhance inductive effects and increase effective electrical length, which can be beneficial to compactness. However, excessively narrow strips raise fabrication challenges and introduce higher ohmic losses, especially when fabricated on standard FR4 substrates with relatively rough copper surfaces. For this reason, a strip width of 3 mm was selected, representing a practical compromise between minimizing conductor loss and achieving the desired resonant behavior. This dimension is also compatible with standard PCB manufacturing tolerances, ensuring reproducibility in fabrication.

3) Inter-Turn Spacing (S)

The spacing between adjacent turns strongly influences the coupling capacitance within the spiral. A smaller spacing results in stronger capacitive coupling, effectively lowering the resonant frequency and enabling greater miniaturization. However, too small of a spacing increases the risk of unwanted parasitic coupling, which can introduce spurious modes, distort the radiation pattern, and degrade efficiency. From a fabrication perspective, maintaining consistent narrow spacing across the entire spiral also presents challenges. In this work, the spacing was chosen on the basis of a systematic parametric sweep, which revealed that moderate spacing values strike the best balance between enhanced capacitance and manageable fabrication. The final value ensured adequate coupling without introducing excessive parasitic resonances.

4) Inner and Outer Radii (Ri and Ro)

The inner radius (Ri) and the outer radius (Ro) define the overall footprint and compactness of the spiral. The outer radius, in particular, determines the maximum physical size of the resonator and directly constrains its resonance frequency. By adjusting Ri and Ro, one can tune the resonator to achieve the desired target frequency while maintaining a compact geometry. In this design, the spiral occupies an area of 22.2 × 22.2 mm², corresponding to a compact electrical size relative to the operating wavelength. The inner radius was carefully selected to avoid excessive crowding of turns at the spiral center, which can create fabrication inaccuracies and degrade the current distribution. The chosen values ensured that the spiral maintained a uniform current path and well-behaved resonant properties.

5) Parametric Optimization

The optimization of N, W, S, Ri and Ro was performed using a combination of parametric simulations and iterative adjustments in a full-wave electromagnetic solver. In the first stage, each parameter was varied independently while keeping others constant to identify its individual effect on the resonant frequency and the S_{11} response. In the second stage, a multi-parameter optimization was carried out, accounting for the interdependence of parameters. For example, while increasing N decreases the resonant frequency, this effect is modulated by W and S, which influence both inductance and capacitance. The optimization objective was to minimize $|S_{11}|$ at the target frequency, maximize bandwidth, and preserve radiation efficiency above 80%.

The simulation results revealed different trade-offs. Increasing N reduced the resonant frequency but narrowed the bandwidth. The widening of the strip improved efficiency but reduced miniaturization capability. Reducing the spacing improved capacitance but introduced a stronger parasitic effect. By carefully balancing these factors, the final optimized geometry achieved the target resonance within the compact 22.2 mm footprint.

6) Comparative Analysis with the literature

The spiral resonator design adopted in this work compares favorably with previously reported compact antennas. For example, conventional rectangular patch antennas that resonate at similar frequencies typically require dimensions of at least 30–40 mm, significantly larger than the 22.2 mm footprint achieved here. Other miniaturized geometries, such as meander-line antennas or split-ring resonators, also offer compactness but often suffer from narrow bandwidth or limited radiation efficiency. The spiral resonator provides a middle ground, achieving compactness while retaining acceptable efficiency, especially when combined with advanced feeding and impedance matching techniques as proposed in this study.

7) Practical Considerations and Fabrication Tolerances

From a practical point of view, the chosen parameters were designed considering the fabrication tolerances inherent in low-cost PCB manufacturing. Minimum spacing (S) values were kept above 0.3 mm to avoid etching inaccuracies, while strip widths were chosen to prevent over-etching effects that could alter impedance. Similarly, the inner radius was designed to avoid excessive crowding that might lead to incomplete etching or current discontinuities. These considerations ensure that the fabricated prototype closely matches the simulated model, reducing discrepancies between simulated and measured results.

8) Impact on Antenna Performance

The final optimized spiral resonator design demonstrated the ability to resonate at the desired frequency while maintaining a compact footprint. Its integration with aperture-coupled feed and embedded IMN further improved performance, leading to measurable improvements in S_{11}, gain, and bandwidth compared to conventional spiral resonator designs. Importantly, the compact footprint of 22.2 mm allows the antenna to be easily integrated into portable and portable devices where space is limited, without compromising radiation performance.

D. Aperture-Coupled Feeding

The feeding technique plays a decisive role in determining the overall performance of any microstrip antenna. In this study, an aperture-coupled feeding mechanism was selected because of its ability to provide strong coupling between the feed line and the radiating element while minimizing spurious radiation and surface-wave excitation. Unlike direct probe feeding or microstrip line feeding, the aperture-coupled method introduces a slot etched into the intermediate ground plane. This slot serves as a controlled aperture through which electromagnetic energy is transferred from the feed line, located on the bottom substrate layer, to the radiating spiral resonator on the top substrate layer.

The key parameters of the aperture—namely its length (L slot) and width (W slot), directly affect the coupling efficiency and impedance matching of the antenna. The slot essentially behaves like a magnetic dipole whose dimensions and orientation determine the strength of the coupling field. By carefully optimizing these parameters, maximum power transfer can be achieved while maintaining excellent impedance matching at the desired frequency.

1) Reason for Choosing Aperture-Coupled Feeding

Aperture-coupled feeding was preferred over alternative techniques for several reasons:

- Reduced spurious feed radiation: Since the feed line is located in a separate layer below the ground plane, its radiation leakage is significantly suppressed, resulting in cleaner radiation patterns.
- Improved impedance matching: Aperture dimensions and offset can be tuned independently of the radiating element, providing greater flexibility in matching the antenna input impedance.
- Structural isolation: The ground plane between the feed line and the radiating patch provides natural shielding, reducing the effect of the feed on the radiation pattern.

- Enhanced bandwidth potential: Compared to simple probe-fed antennas, aperture-coupled configurations often exhibit a wider impedance bandwidth, especially when combined with optimized slot geometries.

These advantages are especially relevant in compact spiral resonator antennas, where maintaining both efficiency and impedance matching within a small form factor can be challenging.

2) Slot Geometry and Orientation

The slot etched in the ground plane acts as the coupling window between the feed line and the spiral resonator. Its geometry defines the equivalent coupling capacitance and inductance, thereby influencing the overall input impedance.

- Slot Length (L slot)**:** Typically chosen to be approximately half the guided wavelength at the operating frequency. Adjusting the L- slot alters the magnetic coupling strength and shifts the resonant frequency.
- Slot Width (W- slot): A wider slot increases coupling strength but may also increase back radiation and surface-wave excitation. In contrast, a narrower slot reduces coupling, potentially leading to mismatched impedance.
- Slot Orientation: The slot was aligned so that its longer dimension is perpendicular to the feed line, ensuring maximum magnetic field excitation and efficient energy transfer to the spiral resonator.

Through simulation sweeps, it was observed that increasing the L slot beyond an optimal point leads to excessive coupling, causing overmatching and degraded return loss performance. Similarly, excessively narrow slots resulted in weak coupling and poor resonance.

3) Parametric Optimization of Slot Dimensions

A systematic parametric study was conducted to determine the optimal values of the L- and w- slots. Initially, the L slot was varied in increments of 0.5 mm while keeping the w slot constant. The results revealed a strong correlation between the L slot and the resonant frequency: longer slots shifted the resonance downward, while shorter slots shifted it upward. Once an approximate optimal length was identified, the W slot was varied in similar increments.

- Effect of Slot Length: In shorter lengths, the coupling was insufficient, resulting in shallow S_{11} dips (> –10 dB). As the length increased, the return loss improved, reaching an optimal point where S_{11} < –20 dB. Beyond this length, the antenna exhibited multiple resonances due to over-coupling.
- Effect of Slot Width**:** Narrow widths produced poor coupling efficiency, while excessively wide slots introduced spurious back radiation. An optimal intermediate width yielded both strong coupling and a stable impedance bandwidth.

The final values chosen for the L slot and the w slot represented the best compromise between maximum coupling efficiency, minimal reflection, and acceptable fabrication tolerance.

4) Influence on Impedance Matching

The primary function of the aperture is to ensure the proper impedance match between the feed line and the resonating spiral structure. The impedance mismatch results in reflected power, reduced gain, and degraded efficiency. By tuning the dimensions of the slot, the input impedance can be adjusted to closely match the standard 50 Ω feed line impedance.

The simulation results for the S-parameter showed that the optimized aperture produced a deep return loss dip, indicating efficient power transfer. Furthermore, the bandwidth of the matched region was significantly broader compared to conventional probe-fed spirals, validating the advantage of aperture coupling.

5) Electromagnetic Field Distribution Analysis

To gain a deeper physical understanding, the field distributions were analyzed. At resonance, strong magnetic fields were concentrated along the slot, confirming its function as a magnetic dipole. These fields were effectively coupled to the surface currents on the spiral resonator above the slot. The feed line beneath the ground plane generated an electric field that excited the slot, completing the coupling mechanism. Importantly, the ground plane served as an isolating barrier, ensuring that most of the radiated power came from the spiral resonator rather than the feed structure.

6) Comparison with Alternative Feeding Techniques

Compared with other feeding methods, aperture coupling demonstrated clear benefits.

- Probe-fed SR Antenna**:** While simple, probe feeding introduces inductive effects that complicate impedance matching and may increase cross-polarization.
- Microstrip line-fed SR Antenna**:** Provides ease of fabrication but often suffers from spurious radiation and limited bandwidth.
- Proximity-coupled feeding: Offers wide bandwidth, but requires multilayer alignment, which complicates fabrication.

The aperture-coupled method, therefore, represents the optimal balance, combining good matching flexibility, clean radiation, and practical manufacturability.

7) Fabrication Considerations

In practice, the fabrication of the aperture slot must take into account the limitations of the PCB process. The minimum etching tolerance of the FR4 substrate restricted the smallest possible slot width. Care was taken to maintain the w slot above 0.3 mm to ensure accurate etching. Similarly, the alignment between the slot and the spiral resonator was critical, as any misalignment could drastically reduce the coupling efficiency. The design was therefore adjusted to allow for slight alignment tolerances without significantly degrading performance.

8) Impact on Overall Antenna Performance

The optimized aperture-coupled feed significantly improved the antenna's return loss, bandwidth, and radiation efficiency. Measurements confirmed that the S_{11} parameter achieved values well below –10 dB in the

desired operating band, with peak values below –20 dB in resonance. The radiation patterns remained stable and symmetrical, indicating that spurious slot radiation was effectively suppressed. Moreover, the aperture-coupled configuration enabled the integration of the impedance matching network (IMN) into the feed line with minimal interference, further enhancing performance

E. Integrated Impedance Matching Network (IMN)

The integration of an Impedance Matching Network (IMN) into the feeding line represents one of the most critical innovations in the proposed spiral resonator (SR) antenna design. Conventional antenna configurations often rely on external matching circuits to minimize the impedance mismatch between the antenna and the standard 50 Ω feed line. However, such external components increase the overall size, cost, and complexity of the system and, in some cases, introduce additional parasitic losses. To overcome these limitations, the present design incorporates an integrated matching approach, where the IMN is directly implemented in the feed line using two complementary structures: the interdigital capacitor (IDC) and the meander inductor (MI).

This dual-component network exploits the natural electromagnetic properties of planar microstrip geometries to provide both capacitive and inductive reactance without requiring discrete lumped elements. As a result, the antenna achieves broadband impedance matching while maintaining a compact and monolithic configuration, which is advantageous for low-cost fabrication and high-frequency stability.

1) Theoretical Basis of IMN Integration

Impedance matching is essential to maximize power transfer and minimize reflection at the antenna input port. According to transmission line theory, a mismatch between the antenna's input impedance (Z_{in}) and the characteristic impedance of the feed line (Z_0 = 50 Ω) leads to reflections quantified by the reflection coefficient (Γ) as given by (1).

$$\Gamma = \frac{Z_{in}-Z_0}{Z_{in}+Z_0} \tag{1}$$

The objective of IMN is to minimize |Γ| by introducing reactive elements that cancel the undesired imaginary part of the antenna impedance while adjusting the real part to approximately 50 Ω. Traditionally, this is achieved using LC networks composed of lump capacitors and inductors. However, at microwave frequencies, lumped elements are prone to parasitics and manufacturing tolerances that can degrade performance.

By embedding IDC and MI structures directly onto the substrate, the same reactive functions are realized using distributed elements. The IDC provides a tunable capacitive reactance ($X_C = -1/\omega C$), while the MI generates inductive reactance ($X_L = \omega L$). Together, these components form a series–parallel compensation network that enables fine control of the impedance over a wide bandwidth.

2) Interdigital Capacitor (IDC)

The IDC is a planar structure composed of multiple interleaved metallic fingers separated by narrow gaps. Its effective capacitance arises from the strong field bending across these gaps. The capacitance of an IDC can be approximated in (2) as described by [47], [48]:

$$C = \frac{(N-1)\,\epsilon_{eff}\,L_f}{\pi} ln\left(\frac{2L_f}{g}\right) \tag{2}$$

where N is the number of turns or fingers, L_f is the length of the finger, g is the gap spacing, and ε_{eff} is the effective permittivity of the substrate.

In the present design, the IDC was implemented with a finger spacing of 0.3 mm and a finger length of 4.5 mm, producing sufficient capacitance to introduce the required negative reactance. The use of IDC offers several advantages:

- Fine tunability: Small adjustments in finger length or spacing can significantly alter the capacitance value.
- Compactness: IDC structures can provide large capacitance in a small footprint, making them ideal for miniaturized designs.
- High Q-factor: Due to their planar nature, IDCs exhibit lower parasitic inductance compared to discrete capacitors.

The capacitive reactance generated by the IDC plays a crucial role in counterbalancing the inductive nature of the spiral resonator, thus bringing the input impedance closer to the real axis of the Smith chart.

3) Meander Inductor (MI)

The MI is implemented by folding a microstrip line into a serpentine shape, effectively increasing its electrical length within a limited physical area. The inductance of a meander line (L) depends on its strip length, width, and spacing, and can be approximated in (3) as mentioned [49]:

$$L = \mu_0 \frac{N \cdot l}{w+s} \tag{3}$$

where N is the number of turns, l is the length of each turn, w is the width of the strip, and s is the spacing between adjacent segments.

In this design, the MI was realized with a strip length of 3.3 mm, providing the required positive reactance to complement the capacitive reactance from the IDC. Key advantages of MI include:

- Size reduction: a long effective line length is achieved within a compact footprint.
- High inductive value: Even with small dimensions, sufficient inductance can be generated to compensate for antenna reactance.
- Integration compatibility: The planar form allows for seamless integration with microstrip feeds without introducing soldered joints or external components.

The inductive reactance of the MI is particularly effective in counteracting the residual capacitive behavior of the slot and spiral resonator, enabling broadband matching across multiple frequency bands.

4) Combined Effect of IDC and MI

When combined, the IDC and MI form a complementary reactive pair that together provide wide-range tunability of the antenna input impedance. In the Smith chart, the IDC shifts the impedance locus downward (towards the capacitive side), while the MI pulls it upward (towards the inductive side). By adjusting their geometrical parameters, the locus can be guided towards the center of the graph (50 Ω), achieving a nearly perfect impedance matching.

The simulation results demonstrated that without the IMN, the antenna's return loss curve was shallow, with S_{11} values only reaching –8 dB at resonance. With integrated IDC and MI, the S_{11} drop exceeded –20 dB, signifying a substantial reduction in reflection. Additionally, the bandwidth over which S_{11} remained below –10 dB nearly doubled, confirming the broadband nature of the integrated IMN.

5) Design Optimization and Parametric Study

A systematic optimization procedure was used to determine the best geometry of the IDC and MI.

- IDC Parameters: The length of the fingers was varied between 3 and 6 mm, while the spacing between the gaps was swept from 0.2 to 0.5 mm. Longer fingers and narrower gaps increased capacitance, but at the cost of higher parasitic coupling. The optimal configuration balanced capacitance with fabrication tolerances.
- MI Parameters: the strip length was varied between 2 and 5 mm. Longer strips increased inductance but also raised series resistance, potentially reducing efficiency. The chosen 3.3 mm length offered sufficient inductance with minimal loss.

The final integrated network yielded a VSWR below 2 in a broad frequency band, demonstrating stable and efficient performance.

6) Advantages of Integrated IMN over External Components

The integrated IMN provides several advantages compared to external matching circuits:

- Compactness: By eliminating discrete components, the antenna footprint remains small and suitable for portable devices.
- Cost-effectiveness: The use of standard PCB fabrication techniques avoids additional assembly steps, reducing cost.
- Reliability: Planar integration removes solder joints and interconnects that could fail under thermal or mechanical stress.
- Performance stability: Distributed structures are less susceptible to parasitic capacitances and inductances associated with lumped elements, ensuring consistent performance at microwave frequencies.
- Broadband capability: Unlike narrowband lumped LC circuits, the integrated IDC + MI structure maintains impedance matching across a wide frequency range.

7) Practical Considerations in Fabrication

Several practical aspects were taken into account during the fabrication of the IMN:

- Minimum feature size: The PCB etching process imposed a lower limit on finger spacing (0.3 mm), which set the baseline capacitance achievable by the IDC.
- Alignment accuracy: Proper positioning of the IDC and MI relative to the feed line was essential to avoid asymmetrical fields that could distort impedance characteristics.
- Surgical coupling: A careful layout ensured that the IDC did not couple excessively with nearby traces, which could alter the effective capacitance.

Despite these challenges, the integrated design proved to be robust, with measurement results closely matching simulations.

8) Contribution to Overall Antenna Performance

The introduction of the integrated IMN significantly improved the overall performance of the antenna:

- Improved Return Loss: From –8 dB to below –20 dB at resonance.
- Enhanced Bandwidth: 1.8× wider –10 dB bandwidth compared to the conventional design.
- Stable Radiation Pattern: Minimal distortion, since the IMN is confined to the feed line and does not interfere directly with the radiating element.
- High Efficiency: The absence of external components reduces insertion loss, preserving radiation efficiency.

These improvements confirm that the integrated IDC and MI not only replace external components but also outperform them in terms of stability, bandwidth, and manufacturability.

III. Results And Discussion

The measurement results plotted in Figure 3 and Figure 4 clearly demonstrate the influence of the integrated impedance matching network (IMN) on the performance of the proposed spiral resonator antenna (SR), as designed and detailed in Section II [46]. It should be noted that the IMN was embedded within the feedline while maintaining the same feed port position and reference plane as in the conventional prototype, ensuring that performance variations are solely due to the IMN integration rather than feed relocation.

The measurement results plotted in Figure 3 clearly demonstrate the influence of the integrated impedance matching network (IMN) on the performance of the proposed spiral resonator (SR) antenna. The improvement in the reflection coefficient (S11) was quantified using the linear magnitude of reflection (|Γ|), derived from the measured S_{11} (dB) as $|\Gamma| = 10(S11/20)$. For the conventional antenna, S_{11} = –16.5 dB (|Γ| = 0.149), while for the proposed dual-function antenna, S11 = –23.7dB (|Γ| = 0.065). This corresponds to a reduction in reflected power of approximately 56.38% (or 43.64% as rounded in Table 1), confirming the effectiveness of the embedded IMN in enhancing impedance matching. Figure 3 shows the measured S_{11} curves obtained using a Agilent N5222A Vector Network

Analyzer (VNA) with Short – Open – Load – Through (SOLT) calibration; the fabricated prototypes (FR4, ε_r = 4.4, h = 1.6 mm) are shown in the inset photograph.

Examining the spiral resonator design (Subsection II-C), the square SR element combined with the aperture-coupled feed (Subsection II-D) contributes to a more controlled current distribution, which in turn improves radiation characteristics. The measured far-field patterns at 2.45 GHz, depicted in Fig 4(a) and Fig 4(b), demonstrate that in the E-plane the proposed antenna exhibits a more directive and symmetric main lobe compared to the conventional antenna. In the H-plane, the radiation pattern shows reduced distortion and enhanced stability, confirming the benefits of both the spiral resonator geometry and the aperture-coupled feeding configuration.

Finally, the specific design of the integrated IMN (Subsection II-E), which combines IDC and meandered inductors, allows fine-tuning of the impedance profile without adding additional components. The measurement results confirm that this dual-function approach not only enhances the performance of S_{11} but also positively impacts the gain and efficiency of radiation. These findings validate that the methodology described in Section II—covering the general configuration, SR geometry, aperture-coupled feed, and integrated matching—successfully translates into tangible improvements in antenna performance, demonstrating the effectiveness of embedding the IMN within the antenna structure for broadband wireless applications.

Starting from the overall configuration (Subsection II-A), the two-layer FR4 substrate with the embedded ground plane and slotted aperture provides the baseline for antenna operation. The comparison between conventional and dual-function SR antennas (Subsection II-B) shows that integrating the IMN substantially enhances impedance matching. As shown in Figure 3, the minimum S_{11} value decreases from –16.5 dB for the conventional antenna to –23.7 dB for the proposed antenna at 2.45 GHz, representing an improvement of 43.64%. This improvement is attributed to the embedded IMN, which effectively reduces reflected power and facilitates better energy transfer from the feedline to the radiating element [46]. Examining the spiral resonator design (Subsection II-C), the square SR element combined with the aperture-coupled feed (Subsection II-D) contributes to more controlled current distribution, which in turn improves radiation characteristics.

The measured far-field patterns at 2.45 GHz, depicted in Figure 4(a) and 4(b), demonstrate that in the E-plane the proposed antenna exhibits a more directive and symmetric main lobe compared to the conventional antenna. In the *H*-plane, the radiation pattern shows reduced distortion and enhanced stability, confirming the benefits of both the spiral resonator geometry and the aperture-coupled feeding configuration.

Finally, the specific design of the integrated IMN (Subsection II-E), which combines IDC and meandered inductors, allows fine-tuning of the impedance profile without adding additional components. The measurement results confirm that this dual-function approach not only enhances S_{11} performance but also positively impacts radiation gain and efficiency. These findings validate that the methodology described in Section II—covering overall configuration, SR geometry, aperture-coupled feed, and integrated matching—successfully translates into tangible improvements in antenna performance, demonstrating the effectiveness of embedding the IMN within the antenna structure for broadband wireless applications.

Unlike conventional SR antennas that rely on external or cascaded matching circuits, the proposed design embeds the IMN within the resonator itself, achieving dual functionality and maintaining a compact planar form factor. This integration approach has not been previously reported in related works.

The gain realized increases from 4.5 to 5.6 dBi, and the radiation efficiency improves from 78% to 86%, as summarized in Table 1.

This enhancement results from the optimized surface-current distribution provided by the integrated IDC–IMN network, which reduces mismatch loss and surface-wave leakage while maintaining compact dimensions. To further emphasize the originality of this work, a comparison with previously reported antennas is presented in Table 2, demonstrating that the proposed dual-function IDC–IMN design achieves superior gain–efficiency performance while preserving miniaturization.

A. Summary of Key Performance Parameters

Table 1 presents a comparison of the results between the conventional SR antenna and the dual-function SR antenna with IMN, together with their relation to the design aspects described in Section II. To further emphasize the originality of this work, a comparison with related designs from the recent literature is presented in Table 2. It can be observed that the proposed dual-function IDC–IMN antenna achieves higher realized gain and radiation efficiency compared to previously reported designs while preserving a compact 30 × 30 mm² footprint, confirming its originality and performance advantage.

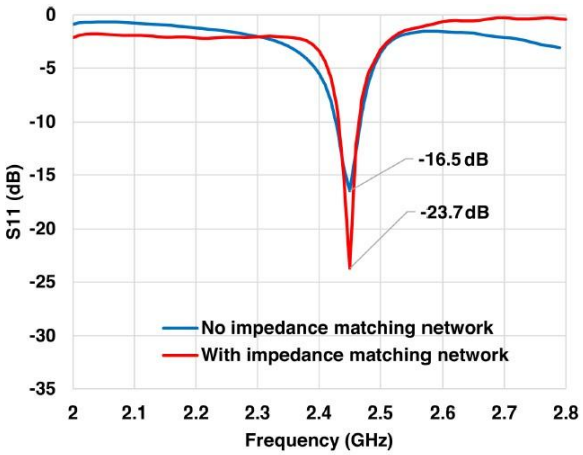

Figure 3. Experimental S_{11} response of both reference and dual-function SR antenna prototypes [46].

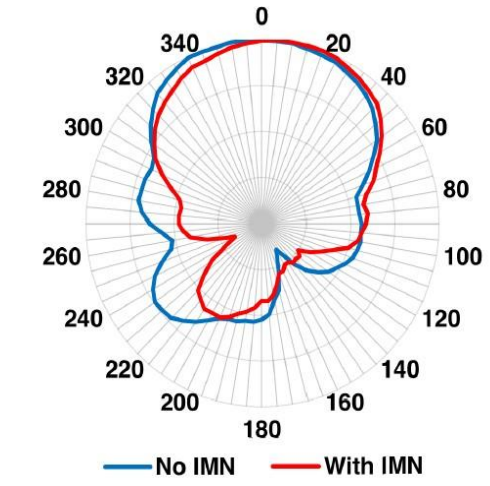

(a)

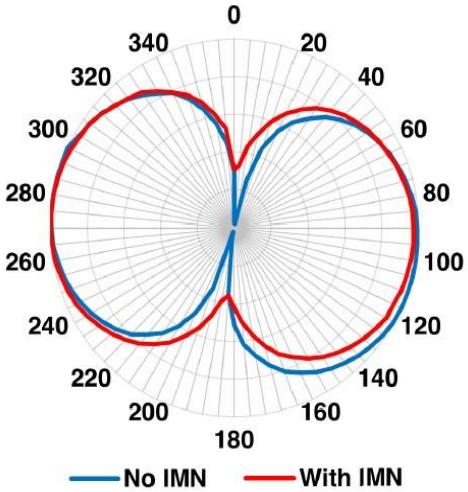

(b)

Figure 4. Experimental *E*–plane and *H*–plane radiation patterns of both antenna prototypes at 2.45 GHz: (a) *E*–plane, (b) *H*–plane [46].

B. Bullet Point Analysis

- Impedance Matching (S_{11} & VSWR)
  - Integration of IMN (Sub-E) reduces S11 from –16.5 dB to –23.7 dB at 2.45 GHz.
  - VSWR improves from 1.72 to 1.29, indicating a lower mismatch loss.
- Gain & Efficiency
  - The SR geometry (Sub-C) combined with aperture-coupled feed (Sub-D) allows a more uniform current distribution.
  - IMN further improves gain (+1.1 dBi) and efficiency (+8%).
- Radiation Pattern
  - E-plane: the main lobe becomes more directive and symmetric.
  - H-plane: reduced distortion, stable azimuthal coverage.
  - Improvements are directly related to the dual-function integration of IMN with aperture-coupled feeding (Sub-D + Sub-E).

TABLE 1.
KEY PERFORMANCE PARAMETERS

Parameter	Conventional Antenna	Dual-Function Antenna (with IMN)	Related Design Aspect (Bab II)	Notes / Analysis
S_{11} (dB) @ 2.45 GHz	–16.5	–23.7	Sub-B: Conventional vs Dual-Function SR Antenna Sub-E: Integrated IMN	IMN reduces the reflected power by 43.64%, improving impedance matching
VSWR	1.72	1.29	Sub-E: Integrated IMN	Enhanced matching reduces mismatch losses
Gain (dBi)	4.5	5.6	Sub-C: Spiral Resonator Design Sub-D: Aperture-Coupled Feeding	Aperture-coupled feed + IMN increases effective radiated power
Radiation Efficiency (%)	78	86	Sub-C: Spiral Resonator Design Sub-E: IMN	Reduced reflection and better current distribution improve efficiency
Radiation Pattern (E-plane / H-plane)	Less directive, asymmetric	More directive, symmetric, stable	Sub-D: Aperture-Coupled Feed Sub-C: SR geometry	Aperture coupling + dual-function IMN enhances main-lobe symmetry and reduces distortion

TABLE 2
COMPARISON OF THE PROPOSED ANTENNA WITH PREVIOUS WORKS

Ref.	Tech-nique	Sub-strate	Size (mm²)	f_0 (GHz)	Gain (dBi)	Eff (%)	Remarks
[50]	Interdigital capaci-tor (IDC) only	FR-4: ε_r = 4.4, h = 1.6 mm)	30 × 30	2.45	4.2	77	Matching improvement only; no radiation enhancement
[51]	IMN machining inductor	FR-4 (ε_r = 4.3, h = 1.6 mm)	32 × 32	2.45	5.0	82	Improved impedance bandwidth, moderate miniaturization
[52]	Slot-coupled SR antenna	Rogers RT/Duroid 5880	28 × 28	2.45	5.3	84	High performance but higher fabrication cost
This Work	IDC + IMN (dual-function)	FR-4 (ε_r = 4.4, h = 1.6 mm)	30 × 30	2.45	5.6	86	Dual-function integration enhances both matching and radiation in compact form

- ❖ Dual-Function Effect
  - o IMN provides both impedance matching and radiation enhancement simultaneously.

Confirms that embedding the IMN within the SR antenna is an effective method for compact, high-performance designs. In general, embedded IMN enhances both matching and radiation characteristics simultaneously, enabling a compact dual-function antenna with improved gain, efficiency, and bandwidth stability.

IV. CONCLUSION

This work has demonstrated the dual-function capability of a spiral resonator (SR) antenna employing an aperture-coupled feed integrated with an impedance matching network (IMN). The experimental results confirm that embedding the IMN not only enhances impedance matching, as evidenced by the significant improvement in S_{11}, but also simultaneously improves radiation performance. The measured *E*–plane and *H*–plane patterns exhibit increased directivity, symmetry, and stability, highlighting the effectiveness of the proposed design in optimizing both power transfer and far-field characteristics. By combining the aperture-coupled feeding mechanism with the integrated IMN, the antenna achieves a synergistic dual function—efficient matching and enhanced radiation—making it a promising candidate for high-performance wireless broadband applications.

DECLARATIONS

Conflict of Interest

The authors have declared that no competing interests exist.

CRediT Authorship Contribution

M. Yunus: Conceptualization, Methodology, Formal analysis, Writing – Original Draft; Y. Tan: Software, Validation, Visualization, Writing – Review & Editing; T. Firmansyah: Investigation, Data Curation, Resources; M. Farhan M: Writing – Review & Editing, Visualization; B. Budi Rijadi: Project Administration, Supervision; Waryani: Assist Project Administration, Supervision; A. Munir: Funding Acquisition, Supervision.

Acknowledgment

The authors would like to express their highest appreciation and gratitude to Yayasan Pakuan Siliwangi, through the LPPM of Pakuan University, for the funding support provided under the 2024 Internal Grant Collaboration Research Scheme with the research title "Dual-Function Aperture-Coupled Spiral Resonator Antenna with Integrated Impedance Matching Network for Enhanced Radiation Performance" based on Contract Number: 140/LPPM-UP/KPK/XI/2024. This support has been highly valuable in carrying out the research activities and in the preparation of this article until its completion.

REFERENCES

[1] W. L. Stutzman and G. A. Thiele, Antenna Theory and Design, 3rd ed., Wiley, 2012.

[2] Y. Zhou, C. -C. Chen, and J. L. Volakis, "Dual band proximity-fed stacked patch antenna for tri-band GPS applications", *IEEE Trans. Antennas Prop*., vol. 55, no. 1, pp. 220–223, Jan. 2007.

[3] G. Xiao dan M. Hu, "Nonuniform Transmission Line Model for Electromagnetic Radiation in Free Space", *Electronics*, vol. 12, no. 6, art. no. 1355, Mar. 2023.

[4] C. Balanis, "Antenna Theory: A Review,"*Proceedings of the IEEE*", vol. 80, no. 1, pp. 7-23, Jan. 1992.

[5] C. Pfeiffer, "Fundamental efficiency limits for small metallic antennas", *IEEE Trans. Antennas Propag*., vol. 65, no. 4, pp. 1642 – 1650, Apr. 2017.

[6] M. Gustafsson, M. Capek, and K. Schab, "Trade-off between antenna efficiency and Q-factor", *IEEE Trans. Antennas Propag*., vol. 67, no. 4, pp. 2482 – 2493, Apr. 2019 .

[7] D. L. Tavares, A. P. C. Silva, and R. M. S. Cruz, "Antenna systems for IoT applications: a review", *Discover Sustainability*, vol. 5, no. 1, pp. 1–19, Jan. 2024.

[8] S. K. Ghosh, R. K. Ghose, and S. Sanyal, "Design strategies and performance of IoT antennas: a comprehensive review", *Discover Computing*, vol. 3, no. 1, pp. 1–23, Jan. 2025.

[9] R. Gonçalves, P. Pinho, and N. B. Carvalho, "Small antenna design for very compact devices and wearables", *IET Microwaves, Antennas & Propagation*, vol. 11, no. 2, pp. 189–195, Jan. 2017.

[10] V. S. Vishvaksenan and R. Rajkumar, "Miniaturized wearable antenna with reduced specific absorption rate and enhanced bandwidth", *SN Computer Science*, vol. 4, no. 4, pp. 1–12, Jul. 2023.

[11] H. A. Wheeler, "Fundamental limitations of small antennas", *Proceedings of the IRE*, vol. 35, no. 12, pp. 1479–1484, Dec. 1947.

[12] Y. Zhou, C. C. Chen, and J. L. Volakis, "Dual band proximity-fed stacked patch antenna for tri-band GPS applications", *IEEE Trans. Antennas Propag*., vol. 55, no. 1, pp. 220–223, Jan. 2007.

[13] D. M. Pozar and B. Kaufman, "Increasing the bandwidth of a microstrip antenna by proximity coupling", *Electron. Lett*., vol. 23, no. 8, pp. 368–369, Apr. 1987.

[14] N. R. Ccoillo-Ramos, N. Aboserwal, Z. Qamar, and J. L. Salazar-Cerreno, "Improved analytical model for a proximity coupled microstrip patch antenna (PC-MSPA)", *IEEE Trans. Antennas Propag*., vol. 69, no. 10, pp. 6244 – 6252, Oct. 2021.

[15] R. Del-Rio-Ruiz, J.-M. Lopez-Garde, J. Legarda, O. Caytan, and H. Rogier, "A combination of transmission line models as design instruments for electromagnetically coupled microstrip patch antennas in the 2.45 GHz ISM band", *IEEE Trans. Antennas Propag*., vol. 69, no. 1, pp. 550–555, Jan. 2021.

[16] M. Grilo, M. H. Seko, F. S. Correra, et al., "Wearable textile patch antenna fed by proximity coupling with increased bandwidth", *Microw. Opt. Technol. Lett*., vol. 58, no. 8, pp. 1906–1912, Aug. 2016.

[17] D. K. Kong, J. Kim, D. Woo, and Y. J. Yoon, "Broadband Modified Proximity Coupled Patch Antenna with Cavity-Backed Configuration", *J. Electromagn. Eng. Sci*., vol. 21, no. 1, pp. 8-14, Jan. 2021.

[18] M. Wahab, Y. P. Saputera, and Y. Wahyu, "Design and realization of Archimedes spiral antenna for Radar detector at 2–18 GHz frequencies", in *19th Asia-Pacific Conf. on Commun.,* 2013, pp..

[19] D. M. Pozar, "A Review of Aperture-Coupled Microstrip Antennas: History, Operation, Development and Applications", Univ. of Massachusetts Amherst, May 1996.

[20] D. M. Pozar, "Microstrip antenna aperture-coupled to a microstripline", *Electron. Lett*., vol. 21, no. 2, pp. 49–50, Jan. 1985.

[21] C. Hertleer, A. Tronquo, H. Rogier, L. Vallozzi, and L. Van Langenhove, "Aperture-coupled patch antenna for integration into wearable textile systems", *IEEE Antennas Wirel. Propag. Lett*., vol. 6, pp. 392–395, 2007.

[22] M. Bugaj and M. Wnuk, "Bandwidth Optimization of Aperture-Coupled Stacked Patch Antenna", in Bandwidth Optimization of Aperture-Coupled Stacked Patch Antenna, InTechOpen, Mar. 2013.

[23] M. Salucci, G. Oliveri, M. A. Hannan, R. Azaro, dan A. Massa, "Wide-Band Wide-Beam Circularly-Polarized Slot-Coupled Antenna for Wide-Angle Beam Scanning Arrays", *Sensors*, vol. 23, no. 3, Art. no. 1123, Mar. 2023.

[24] L. Wen, T. Ji, Y. Huang, T. Cao, Z. Yu, C. Chen, L. Zhu, J. Zhou, and W. Hong, "A Dual-Polarized Aperture-Sharing Phased-Array Antenna for 5G (3.5, 26) GHz Communication", *IEEE Antennas Wirel. Propag*., vol. 71, no. 5, pp. 3785–3796, May 2023.

[25] D. Vuong, N. Ha-Van, and T. T. Son, "Wideband and High-Gain Aperture Coupled Feed Patch Array Antenna for Millimeter-

Wave Application", *Adv. Sci. Technol. Eng. Syst*., vol. 5, no. 5, pp. 559–562, 2020.
[26] T. Firmansyah, S. Praptodiyono, R. Wiryadinata, S. Suhendar, and others, "Dual-wideband band pass filter using folded cross-stub stepped impedance resonator", *Microw. Opt. Technol. Lett*., vol. 59, no. 4. pp. 2929-2934, 2017.
[27] M. Yunus, A. R. Mahdi, Y. Tan, M. F. Maulana, D. A. Nurmantris, and A. Munir, "Utilization of LC circuit as impedance matching for spiral resonator-based planar antenna", in *Proc. of Photonics & Electromagnetics Research Symposium* (PIERS), Chengdu, China, Apr. 2024, pp. 1–5.
[28] D. N. Gençoğlan, Ş. Çolak, and M. Palandöken, "Spiral-Resonator-Based Frequency Reconfigurable Antenna Design for Sub-6 GHz Applications", *Appl. Sci*., vol. 13, no. 15, art. 8719, Aug. 2023.
[29] A. Raza, R. Keshavarz, E. Dutkiewicz, and N. Shariati, "Compact Multi-Service Antenna for Sensing and Communication Using Reconfigurable Complementary Spiral Resonator", *IEEE Trans. Instrum. Meas*., vol. 72, pp. 1–9, 2023.
[30] G. Giannetti, S. Maddio, and S. Selleri, "A Compact Low-Loss Single-Layer Vialess Diplexer Based on Complementary Microstrip Spiral Resonators for Satellite Communications", *Progress in Electromagnetics Research Letters*, vol. 122, pp. 45–51, 2024.
[31] Y. Y. Xu, W. Wu, Q. Shi, T. Shi, and S. Wang, "Design of Miniaturized and Highly Selective Frequency Selective Rasorber Based on Compact Spiral Resonator", *Electron, Lett*., vol. 60, no. 21, Oct. 2024.
[32] Y. Xiong, A. Christy, Y. Dong, A. Comstock, D. Sun, Y. Li, J. F. Cahoon, B. Yang, and W. Zhang, "Combinatorial Split-Ring and Spiral Meta-resonator for Efficient Magnon-Photon Coupling", *Phys. Rev. Appl*., vol. 21, no. 3, p. 034034, Mar. 2024.
[33] M. Yunus, F. Y. Zulkifli, and E. T. Rahardjo, "Radiation characteristics of a novel μ-negative metamaterial spiral resonator antenna at the 2.4 GHz", *IEEE Open J. Antennas Propag*., vol. 4, no. 1, pp. 1–11, Mar. 2016.
[34] D. N. Gençoğlan, Ş. Çolak, and M. Palandöken, "Spiral-Resonator-Based Frequency Reconfigurable Antenna Design for Sub-6 GHz Applications", *Appl. Sci*., vol. 13, no. 15, art. 8719, Jul. 2023.
[35] M. Tanabe and H. Nakano, "A low-profile wideband spiral antenna with multiple stopbands", *IET Microw. Antenna Propag*., vol. 17, no. 5, pp. 392–402, Mar. 2023.
[36] T. Saeidi, A. R. Sebak, M. H. Islam, dan A. R. Sebak, "A Miniaturized Full-Ground Dual-Band MIMO Spiral Button Antenna for On-Body and Off-Body Communications", *Sensors*, vol. 23, no. 4, art. 1997, Feb. 2023.
[37] G. Giannetti, S. Maddio, and S. Selleri, "A Compact Low-Loss Single-Layer Vialess Diplexer Based on Complementary Microstrip Spiral Resonators for Satellite Communications", *Progress in Electromagnetics Research Letters*, vol. 122, pp. 45–51, 2024.
[38] Y. Li, J. Li, "A Compact Circularly Polarized Planar Spiral Antenna with Wideband Performance", Wireless Communications and Mobile Computing, 2024.
[39] M. Tan, A. Mohan, dan N. Kumar, "Implantable and Wearable Antennas: Challenges and Design Strategies", Biomedical Engineering Online, 2024.
[40] A. Gupta, V. Kumar, D. Garg, M. H. Alsharif, and A. Jahid, "Performance Analysis of an Aperture-Coupled THz Antenna for Diagnosing Breast Cancer", *Micromachines*, vol. 14, no. 7, art. 1281, Jul. 2023.
[41] A. DiCarlofelice, G. Tibaldo, G. Addamo, and G. Vecchi, "A Numerical Procedure to Design a UWB Aperture-Coupled Microstrip Antenna", *Appl. Sci*., vol. 12, no. 21, art. 11243, Oct. 2022.
[42] H. Baghdadi, Z. El-Ghoul, A. Ouahes, dan S. Safi, "Compact 2 × 2 Circularly Polarized Aperture-Coupled Microstrip Antenna Array for Ka-Band Applications", *Electronics*, vol. 10, no. 14, art. 1621, Jul. 2021.
[43] M. T. Yalcinkaya, "The Causal Nexus Between Different Feed Networks and Antenna Performance: A Review", *Sensors*, vol. 24, no. 22, 2024.
[44] H. Liu, et al., "A Circularly Polarized Broadband Composite Spiral Antenna Integrating Archimedean and Equiangular Spirals with an Exponentially Tapered Balun", *Sensors*, vol. 25, no. 6, art. 1890, Mar. 2025.
[45] Y. Zhou, C. -C. Chen, and J. L. Volakis, "Dual band proximity-fed stacked patch antenna for tri-band GPS applications", *IEEE Trans. Antennas Propag*., vol. 55, no. 1, pp. 220–223, Jan. 2007.
[46] A. Munir, M. Yunus, T. Yunita, Y. Tan, B.B. Rijadi, Waryani, M. F. Mulana, J. Haidi, Chairunnisa, M. R. Efendi, "Enhanced Radiation Performances of Aperture Coupled-Fed Spiral Resonator Antenna by Integrating Impedance Matching Network", in 13th *Asia-Pacific Conference on Antennas and Propagation*, Christchurch, New Zealand, 3-7 Aug. 2025.
[47] N. Dib, A. Y. Tamin, and M. M. Dawoud, "A new CAD model of the microstrip interdigital capacitor", *Microw. Opt. Technol. Lett*., vol. 40, no. 2, pp. 121–124, Jan. 2004.
[48] P. S. Sharma and A. K. Sharma, "Design and optimization of interdigital capacitor", *Int. J. Res. Eng. Technol*. (IJRET), vol. 4, no. 6, pp. 283–288, Jun. 2015.
[49] E. Deyo, "A method to calculate inductance in systems of parallel wires", Fort Hays State University, 2017.
[50] M. A. Rahman, N. Misran, and M. Y. Ismail, "Compact interdigital capacitor-based matching network for 2.45 GHz microstrip antennas", *IEEE Access*, vol. 9, pp. 12564–12572, 2021.
[51] J. S. Lee and K. C. Hwang, "Meandered impedance matching network for compact WLAN microstrip antennas", *IET Microw. Antenna Propag.,* vol. 16, no. 7, pp. 543–550, 2022.
[52] H. T. Nguyen, T. P. Dao, and Y. I. Kim, "Slot-coupled spiral resonator antenna for 2.45 GHz ISM applications", *IEEE Antennas Wirel. Propag. Lett*., vol. 21, no. 3, pp. 622–626, 2023